Carbon Quantum Dots Hot Paper

How to cite: *Angew. Chem. Int. Ed.* **2022,** *61,* e202211365
International Edition: doi.org/10.1002/anie.202211365
German Edition: doi.org/10.1002/ange.202211365

Supramolecular Assembly of Edge Functionalized Top-Down Chiral Graphene Quantum Dots

Mikiko Vázquez-Nakagawa, Laura Rodríguez-Pérez, Nazario Martín, and M. Ángeles Herranz**

Dedicated to Prof. Miguel A. Alario on the occasion of his 80th birthday

Abstract: The construction of supramolecular assemblies of heterogeneous materials at the nanoscale is an open challenge in science. Herein, new chiral graphene quantum dots (GQDs) prepared by amidation reaction introducing chiral amide groups and pyrene moieties into the periphery of GQDs are described. The analytical and spectroscopic data show an efficient chemical functionalization and the morphological study of the supramolecular ensembles using SEM and AFM microscopies reveals the presence of highly ordered fibers of several micrometers length. Fluorescence studies, using emission spectroscopy and confocal microscopy, reveal that the fibers stem from the π-π stacking of both pyrenes and GQDs, together with the hydrogen bonding interactions of the amide groups. Circular dichroism analysis supports the chiral nature of the supramolecular aggregates.

Introduction

Carbon is one of the 92 natural elements in our planet, constituting the 0.1 % of Earth crust. This chemical element, known and used by Egyptians and Sumerians, has been associated to the humankind's progress. Recently, this element has been the focus of extensive research, following the discovery of new allotropes exhibiting amazing nanoforms. Among this vast family of carbon nanostructures, two-dimensional (2D) graphene—which is formed by a one-atom thick honeycomb lattice of sp^2 carbon atoms—has attracted tremendous attention because of its promising mechanical, thermal, optical and electronic properties.[1] However, 2D pristine graphene is a semimetal of zero band gap which prevents its use in opto-electronic applications where a suitable band gap is required.[2] In contrast, graphene quantum dots (GQDs), known as zero-dimensional (0D) nanomaterials, exhibit a variety of opto-electronic properties, including fluorescent, photoluminescent and chemiluminescent properties, which make them attractive materials for different practical purposes.[3] Compared to graphene layers, GQDs are graphene nanosheets with lateral dimensions of <100 nm in single-, double- and few- (3 to <10) layers.[4] Associated with their nanostructure, these GQDs have quantum confinement and edge effects exhibiting photo-luminescence emission.[5]

Two main approaches have been exploited to synthesize GQDs, the *bottom-up*[6] (through organic synthesis) and *top-down*[7] (cutting off graphene sheet). In both cases, the resulting materials have demonstrated a great potential in bio-imaging devices,[8] sensors,[9] photocatalysts,[10] and light-emitting devices.[11] More recently, GQDs films have also been used for the fabrication of perovskite solar cells.[12]

In the last few years, many efforts have been paid in optimizing the synthetic methods and doping for enhancing the GQDs fluorescence. However, just a few studies deal with the formation of macro-scale structures of GQDs in solid state.[13] As presented recently, GQDs can assemble into mesoscale chains, sheets, supraparticles, nanoshells and nanostars by coordination interactions with metal ions commonly present in the environment.[14] Self-assembly has also become a reliable approach to synthesize stacks of GQDs with important levels of structural complexity.[15] By the introduction of hydrogen-bonding synergistic functional groups, a sophisticated supramolecular GQD-containing polymer network was reported by Haino and co-workers, thus showing that GQDs can be used as a platform for supramolecular self-assembly, thus opening up new avenues for the design of supramolecular polymers by suitable chemical functionalization.[16]

Chirality is a fascinating property of interest in natural products and materials science which, however, has scarcely been applied in carbon nanostructures.[17] In this regard, chiral GQDs have mainly been synthetized by *bottom-up* methodologies with a great variety of molecular topologies

[*] M. Vázquez-Nakagawa, Dr. L. Rodríguez-Pérez, Prof. Dr. N. Martín, Prof. Dr. M. Á. Herranz
Department of Organic Chemistry, Faculty of Chemistry, Universidad Complutense de Madrid
28040 Madrid (Spain)
E-mail: nazmar@ucm.es
maherran@ucm.es
Prof. Dr. N. Martín
IMDEA-Nanociencia
c/Faraday 9, Campus Cantoblanco, 28049 Madrid (Spain)

and properties.[18] In contrast, only limited examples of chiral *top-down* GQDs have been reported so far.[19] In 2016, we proved that GQDs obtained from pristine graphene sheets could become chiral.[20] The GQDs covalent functionalization with enantiomerically pure (*R*) or (*S*)-2-phenyl-1-propanol leads to the formation of chiral GQDs. Applying this strategy, we were able to transfer chirality to a supramolecular structure built with pyrene molecules. The circular dichroism of the chiral GQDs/pyrene ensembles shows a characteristic chiroptical response depending on the configuration of the organic ligands anchored. Going one step further, Haino et al. attached chiral phenylethyl and *p*-bromophenylethyl groups onto the GQDs edges generating chirality on the GQDs surface. The dichroic signal observed is related with a transfer of chirality from the organic addend to the GQDs surface edges through steric interactions.[21]

Based on these simple approaches, in the present study we explore the construction of sophisticated chiral carbon-based GQDs supramolecular organizations. We demonstrate that GQDs covalently modified with a pyrene chiral derivative self-organize onto a chiral nanostructured material, showing that it is possible to implement and transfer the chiral information.

Results and Discussion

The synthetic strategy for obtaining the new hybrid materials has been developed as follows: GQDs were obtained from graphite oxide (GO) previously synthetized using Hummers method.[22] Briefly, GO was submitted to a mild oxidative cutting in a mixture of H_2SO_4 and HNO_3 (3/1 v/v) at 120 °C for 48 h. The solution was subsequently neutralized and dialyzed for obtaining water soluble GQDs (for further experimental details, see Supporting Information). Thermogravimetric analysis (TGA) was performed to determine the thermal-decomposition profile of GO, and GQDs in an inert atmosphere (100–700 °C). As shown in Figure S9, GO presents a weight loss of 33 % compared to GQDs which presents a 45 %. This huge difference could be related to a higher rate of oxygenated groups on the GQDs edges together with a size decrease. In fact, the diameter size measured using transmission electron microscopy (TEM) and analyzed through a histogram could be estimated in 4.8 ± 0.9 nm (Figure S10).

In the ^{13}C NMR spectrum of GQDs, measured in D_2O, characteristic signals at 134.5 and 130.1 ppm, due to the presence of sp^2 graphitic carbon, and the signal of carboxylic acids at 172.4 ppm are observed, as reported in the literature.[23] The FTIR spectrum of GQDs showed a wide band corresponding to the O–H stretching vibration at 3450–3430 cm^{-1}, stretching vibrations of C=O at 1721–1714 cm^{-1}, and the band due to vibrations in-plane of C=C observed at 1595 cm^{-1}. The UV/Vis absorption spectrum recorded for GQDs shows a broad absorption peak at ≈230 nm characteristic of this kind of materials (Figure S13).[24]

The new **GQDs-1(*R*)** and **GQDs-1(*S*)** materials were prepared by following a multistep synthetic procedure. First, the synthesis of the enantiomerically pure molecule **1(*R*)/(*S*)** was achieve by an esterification reaction between Fmoc-Ala-OH and 1-pyrenebutanol in the presence of *N,N′*-dicyclohexylcarbodiimide (DCC) and 1,4-dimethylpyridinium *p*-toluenesulfonate (DPTS). The use of acid-base extraction in a second step provides the stable salts of the desired products. The edge-functionalization of GQDs with **1** is outlined in Scheme 1.

GQDs were refluxed with thionyl chloride for 24 h to convert the carboxylic acid groups to acid chlorides. The reaction mixture was *in situ* subjected to an amidation reaction with **1(*R*)** or **1(*S*)** in a mixed solution of DMSO and triethylamine at 120 °C for 48 h. Purification of the samples was carried out easily. Initially a precipitation step in cold diethyl ether followed by centrifugation and washing with methanol was carried out. In a subsequent step, washing in dichloromethane removed the excess of free **1(*R*)** or **1(*S*)** molecules. The enantiomerically pure amides obtained result in chiral graphene quantum dots. Nevertheless, it is well-known that π-π stacking interactions between the sp^2 surface of aromatic honeycombs of GQDs and pyrene moieties could lead to the non-covalent functionalization of these materials.[25] In order to exclude this possibility, we have carried out the supramolecular functionalization of GQDs with the prepared pyrene derivatives **1(*S*)** and **1(*R*)**, and compared the aggregates thus formed with the covalent derivatives **GQDs-1(*R*)** and **GQDs-1(*S*)**. The protocols to form the supramolecular hybrids were developed—see experimental procedure for details.

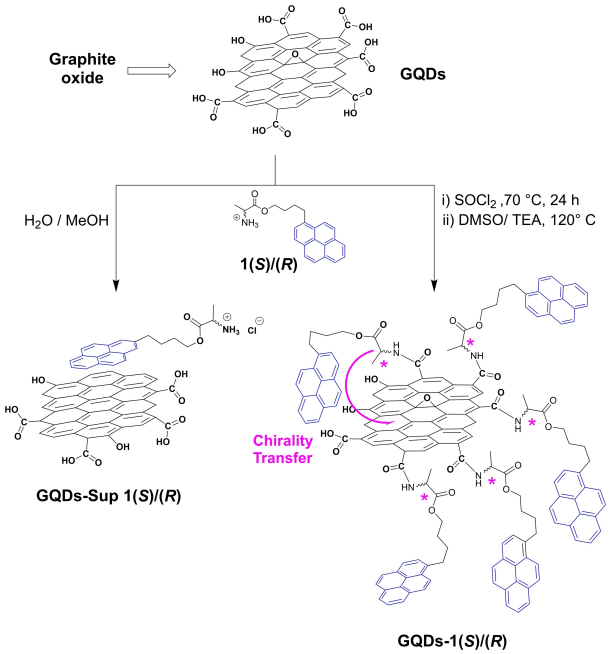

Scheme 1. Schematic representation of the synthesis of chiral **GQDs-1(*R*)** and **GQDs-1(*S*)** by amidation reaction with compound **1(*R*)** or **1(*S*)**.

The successful introduction of the pyrene-amino group was primarily evidenced using TGA analyses (Figure 1 and Figure S11). The thermogravimetric profiles of **GQDs-1(*R*)** and **GQDs-1(*S*)** present a thermal stability with a weight loss of around 51 and 59 %, respectively, at 370 °C. Therefore, it was estimated that around 25–35 pyrene molecules functionalized the GQDs periphery (see the Supporting Information for details about the calculations). No sight of weight loss around 200 °C is observed for the functionalized derivatives, attributed to the decomposition of carboxylic acid groups at the edges of the GQDs. This suggests an almost complete functionalization of the carboxylic acid functionalities. In contrast to the covalent derivatives, both **GQDs-sup 1(*S*)/(*R*)** present a first decomposition profile of pristine GQDs carboxylic acid functionalities around 200 °C. Additionally, the second weight loss of the decomposition profile of **1(*R*)/1(*S*)** is noticed at around 370 °C. This finding was assigned to the removal of the pyrene derivative moieties anchored to the GQDs core by π-π stacking interactions. The weight loss found was 27 % for **GQDs-sup 1(*S*)** and 23 % for **GQDs-sup 1(*R*)**. As expected, the supramolecular functionalization of GQDs is lower compared to the covalent functionalization, with approximatively 10–15 **1(*R*)/1(*S*)** molecules on the GQDs surface. Analyzing the results, we can conclude that **GQDs-sup 1(*R*)/(*S*)** present a lower level of functionalization compared to **GQDs-1(*R*)** and **GQDs-1(*S*)**. The small size of our GQDs and a high oxidation degree, providing numerous available -COOH units in their periphery, might be the reason of such a different level of functionalization.

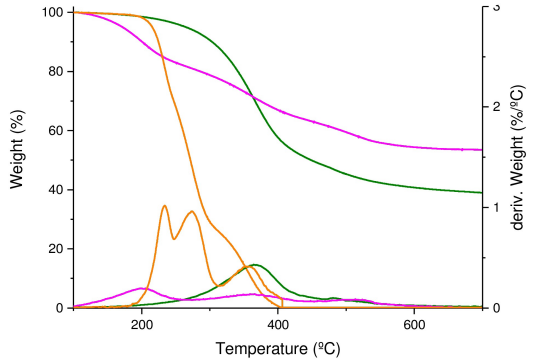

Figure 1. TGA comparative analysis of **GQDs-1(*S*)** (green) vs. the supramolecular assemblies **GQDs-sup 1(*S*)** (magenta) and compound **1(*S*)** (brown).

The FTIR spectra of functionalized **GQDs-1(*R*)/(*S*)** clearly confirm the covalent linkage to the GQDs core. Thus, the C=O stretching vibrations of the carboxylic group at 1721–1714 cm^{-1} disappears, together with the appearance of two C=O bands at 1668 cm^{-1} (amide) and 1737 cm^{-1} (ester) (Figure 2). As expected, the FTIR spectra of the functionalized GQDs is very similar to the non-functionalized GQDs, showing the characteristic bands of the C=O corresponding to the carboxylic acid groups on the edge of GQDs and ester groups present in the free molecules [**1(*R*)** or **1(*S*)**] with no signatures of the amide groups.

X-ray photoelectron spectroscopy (XPS) allowed the observation of all the elements present in the samples. The full scan spectra for **GQDs-1(*R*)** and **GQDs-1(*S*)** exhibit the signals for C 1s (284.6 eV), O 1s (532.6 eV) and N 1s (399.6 eV) (Figure 3 and Figure S12). The C 1s energy level was deconvoluted using five Gaussian-Lorentzian curves. The main component centered at 284.4 eV is assigned to (C=C)/C–C. The subsequent minor components localized around 284.9, 285.5 and 286.5 eV are related to carbon atoms bounded to heteroatoms in different oxidation states assignable to C–O/C–N, C–O–C and C=O. The last component around 290 eV corresponds to the π-π* shake up.[26] Interestingly, the XPS survey spectra of **GQDs-sup 1(*R*)/(*S*)** provides the exact same location for C 1s (284.6 eV) and O 1s (532.6 eV) peaks. The N 1s core is found shifted to a higher binding energy (401.6 eV), which is consistent with a supramolecular interaction between the GQDs and the molecule **1(*S*)**, where the N atom remains as a quaternary amine (inset in Figure 3 and Figure S12).

The UV/Vis absorption and fluorescence spectra of the chiral hybrids **GQDs-1(*R*)** and **GQDs-1(*S*)** compared with the supramolecular **GQDs-sup 1(*R*)/(*S*)** are shown in Figure 4. In the UV/Vis spectra, both types of functionalized

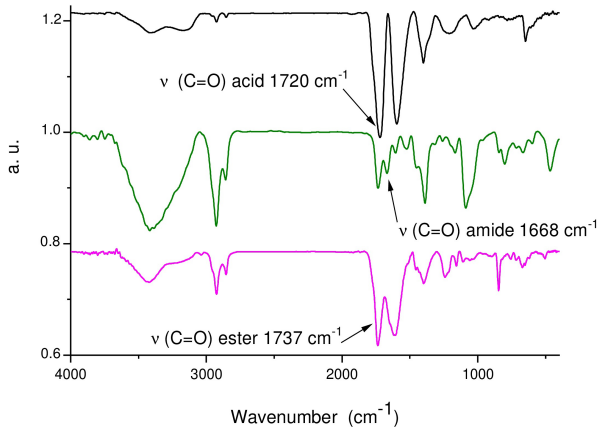

Figure 2. FTIR spectra of GQDs (black), **GQDs-1(*S*)** (green) and **GQDs-sup 1(*S*)** (magenta).

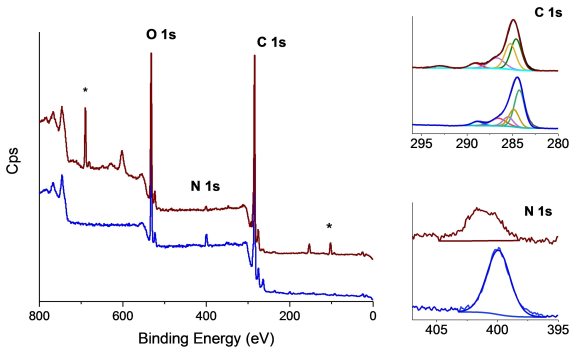

Figure 3. XPS survey spectra of **GQDs-1(*R*)** (blue) and **GQDs-sup 1(*R*)** (brown). The insets detail the C 1s and N 1s peaks deconvolutions. Highlighted with an asterisk are the XPS peaks of Si 2p (102.5 eV) and F 1s (690.5 eV) from the sample holder.

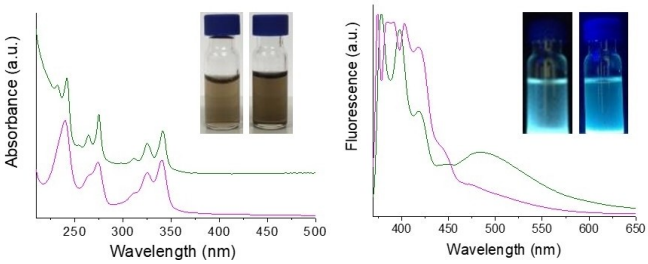

Figure 4. Absorption spectra (left) at daylight, and emission spectra (right) under 365 nm excitation wavelength, of the covalent aggregate **GQDs-1(*S*)** (green) compared to the supramolecular material **GQDs-sup 1(*S*)** (magenta) in CH_3OH/H_2O (1:1). The UV/Vis solutions have a concentration of 0.30 g L^{-1} for both **GQD-1(*S*)** and **GQD-sup 1(*S*)**. The PL was registered for solutions of 0.15 g L^{-1} for **GQD-1(*S*)** and **GQD-sup 1(*S*)**. The inset photographs correspond to **GQDs-sup 1(*S*)** and **GQDs-1(*S*)** solutions (from left to right) in CH_3OH/H_2O (1:1).

GQDs show, as expected, the typical absorption in the entire visible region of GQDs related to sp^2 graphene honeycombs (Figure S13). The pyrene bands for **1(*R*)/(*S*)** (Figure S14) are observed for both **GQDs-1(*R*)/1(*S*)** and **GQDs-sup 1(*R*)/(*S*)**. Interestingly, the absorption features of the pyrene molecule in **GQDs-sup 1(*R*)/(*S*)** experience a small blue shift (ca. 2 nm) when compared to **1(*R*)/(*S*)** or **GQDs-1(*R*)/1(*S*)**, which could be accounted for by the π-π interactions of pyrene fragments with the GQDs skeleton.[27] On the other hand, the fluorescent emission spectra of the pyrene derivatives are characterized by an assembly of well-defined bands between 375 and 410 nm referred as the monomer bands. A second notable feature of pyrene fluorescence emission is a broad band at longer wavelengths, ranging from 425 to 550 nm, when two pyrene rings are ≈10 Å from each other. The long lifetime of pyrene emission (>100 ns), allows the appearance of this excitation state or excimer involving the interaction between two pyrenes.[28] The photoluminescence spectra (λ_{exc} = 365 nm) of all GQDs derivatives exhibit the characteristic emission of pyrene fragments. An unstructured excimer band was surprisingly found while recording the spectra of the covalent hybrids **GQDs-1(*R*)** and **GQDs-1(*S*)** and it is centered at 485 nm (Figure 4). This fact may involve interactions between, at least two pyrene rings that are spatially proximal to each other, maybe in an intermolecular context. However, the PL spectra of the supramolecular aggregates do not present the excimer band, indicating a disruption of the supramolecular interaction among the pyrene rings replaced by a pyrene-GQDs interaction.

As we have recently reported, the chiroptical properties of chiral GQDs could be investigated by circular dichroism (CD).[20] In our previous work, the chiral moieties covalently attached to the GQDs surface did not have any obvious absorption over 300 nm. The addition of pyrene to the studied chiral GQDs solution aid the formation of supramolecular assemblies, which could trigger the chiral properties by means of π-π stacking forces. As expected, the pyrene/chiral GQDs solutions displayed an obvious CD signal. The pyrene inclusion as part of the chiral residue connected to the GQDs, allows the dichroic response study of this new chiral GQDs in a straightforward manner. In particular, **GQDs-sup 1(*S*)** revealed a positive Cotton effect in the absorption range of 320–350 nm, specifically at the pyrene absorption bands, while those GQDs containing the enantiomerically pure *R* units, **GQDs-sup 1(*R*)**, showed the opposite negative Cotton effect in the same absorption range (Figure 5a). In control experiments, DMSO solutions of **1(*R*)/(*S*)** present almost the same CD response with positive/negative Cotton effect at the pyrene absorption bands (Figure S15).

Moving forward to the covalent aggregates, the CD assays for **GQDs-1(*S*)** in DMSO (Figure 5b) led to a bisignate signal with a high negative Cotton effect in the absorption range of 200–270 nm, a positive Cotton effect between 270–350 nm and an almost zero cross point at 270 nm. As expected, **GQDs-1(*R*)** showed the opposite Cotton effect with the equivalent zero cross point in the same absorption range. This chiroptical response in the range of GQDs absorption supports a chirality transfer from the organic molecule to the GQDs supramolecularly assembled.[29] In both cases, the small differences in the CD signals of the *R*- and *S*-chiral GQDs aggregates could be related with the non-identical size, surface functionalization and organization.

Graphene quantum dots have aromatic surfaces capable of stacking by means of efficient π-π interactions. When a chiral molecule like **1(*R*)** or **1(*S*)** is anchored to the edges of GQDs, the hydrogen bonding of the amide-group and the pyrene π-π interactions also play a key role on their supramolecular arrangement. Hence, the recorded scanning electron microscopy (SEM) images of **GQDs-1(*R*)/1(*S*)** (Figure 6 and Figure S16) reveal that the precipitates have a fiber like morphology of several micrometers long with a variable thickness. Figure 6 shows how these fibers are twisted at some point along their main axis. Possibly, the enantiomerically pure character of the chiral GQDs might be the responsible of the fiber rotation for both enantiomers, even though no helicoidally homogeneity was found. At this point, it is important to remark that it is difficult to correlate chirality with the nanostructure obtained, particularly when dealing with heterogeneous materials. SEM images recorded for the supramolecular aggregates do not form any supramolecular assembly as expected (Figure S17).

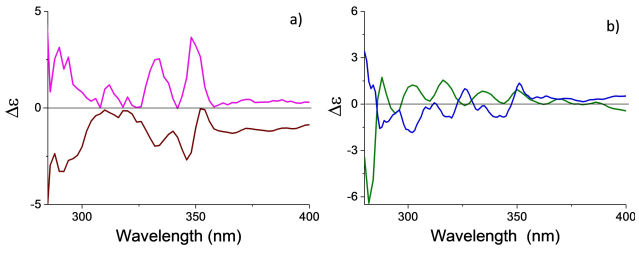

Figure 5. a) Circular dichroism spectra in DMSO for the supramolecularly assembled **GQD-sup 1(*R*)** (brown) and **GQD-sup 1(*S*)** (magenta). b) Circular dichroism spectra in DMSO for aggregates **GQD-1(*R*)** (blue) and **GQD-1(*S*)** (green). All samples were measured with a concentration of 0.1 g L^{-1}.

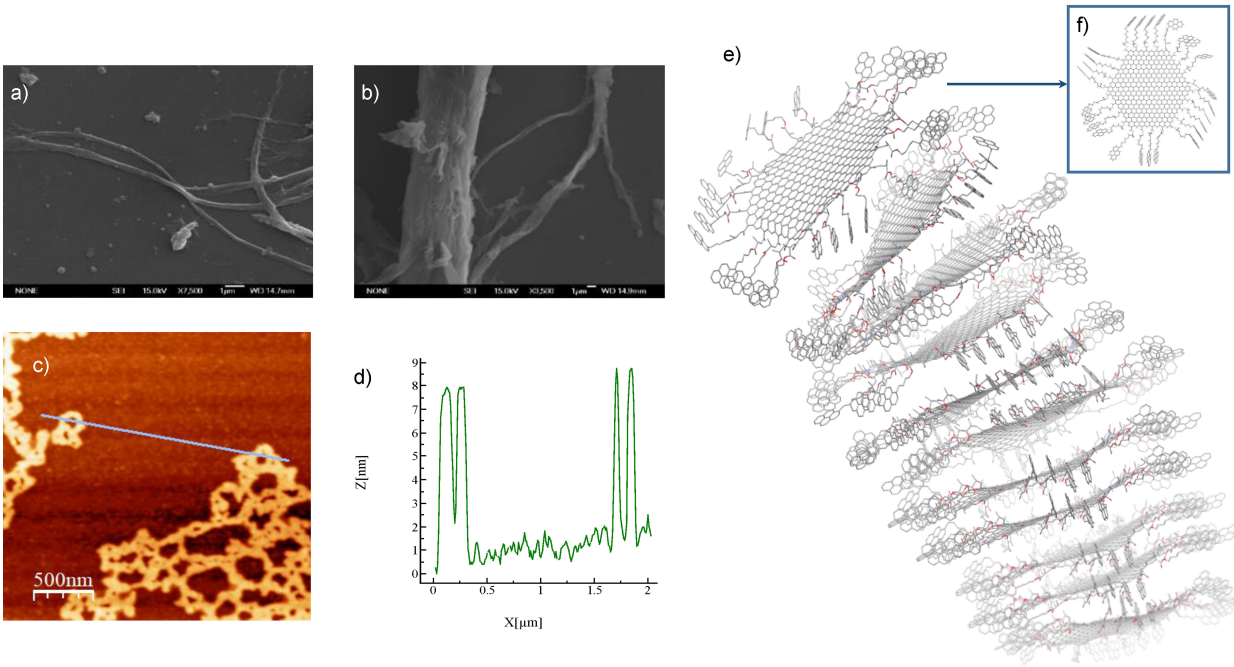

Figure 6. a) SEM images of **GQDs-1(*R*)** at ×3500 and b) ×500 magnifications. c) AFM image of **GQDs-1(*R*)** and d) height profile of the fibers formed (from left to right). e) Schematic illustration of the process of the aggregation constructing a fiber like structure. f) Structure of the **GQDs-1(*S*)** monomer with size of 70.9×67.0 Å^2. Carbon atoms are represented in grey, oxygen atoms in red and nitrogen atoms in blue. Hydrogen atoms are excluded from the structure to simplify the design.

The straight needles shape structure of **1(*S*)** and **1(*R*)** is also provided in the Supporting Information (Figures S18 and S19) as a blank.

Detailed morphological studies by AFM were obtained to further understand the inner structure and formation of **GQDs-1(*R*)/1(*S*)** fibers and elucidate the specific interactions along the stacking. In Figure 6, it is observed that **GQDs-1(*S*)** forms relatively homogeneous and long polymeric assemblies of around 12–14 nm height and entangled with each other. Similar results emerge when studying the pseudo-enantiomer material **GQDs-1(*R*)** (Figure S20). Pristine GQDs showed a dotted morphology as reported in the literature, with a flat disposition of few multi-layers GQDs.[21] Therefore, morphologically, this supramolecular structures are unique and uniform throughout the entire images, in an arrangement driven by the π-π aromatic interaction between GQDs honeycombs and pyrene-pyrene, and the hydrogen bonding between amides (Figure 6e–f). The FTIR relatively blue shifted and broad bands of the amide carbonyl group (1668–1672 cm^{-1}) in **GQDs-1(*R*)** and **GQDs-1(*S*)** are a good evidence of the hydrogen bonding between them.[30] As fluorescent nanomaterials with biocompatibility, GQDs show enormous potential for fluorescent bioimaging.[31] Confocal microscopy images of **GQDs-1(*R*)/1(*S*)** fibers were obtained at 405 nm excitation wavelength showing high stability upon light irradiation (Figure 7, Figure S21). The fluorescent emission of **GQDs-1(*S*)** is split in two different regions, first the GQDs subunit at 652–780 nm (red emission) and the second and more intense, corresponding to the pyrene derivative **1(*S*)** at 410–520 nm (green emission) (Figure S22). The overlay of both images leads to a fiber with lesser red emission on their center surrounded by a bright green fluorescent. This result is consistent with the hypothesis of assemblies with a central GQDs core surrounded by the organic pyrene moieties. Some isolated red color can also be observed due to the emission of the less functionalized GQDs. The steady state fluorescence of GQDs in water evidences a tailing emission up to 800 nm (Figure S23).

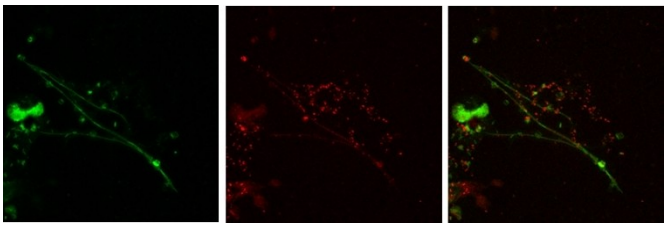

Figure 7. Fluorescence microscopy images of **GQDs-1(*S*)** collected upon excitation at 405 nm in two channels, one at 410–520 nm (green emission, left) corresponding to emission of the pyrene derivative molecule and the other at 652–780 nm (red emission, centred) corresponding to emission of GQDs. The overlay of the separated channels is shown in the right panel.

Conclusion

In summary, the present study shows the potential of GQDs as building blocks for the construction of supramolecular

polymers at the nanoscale. Enantiomerically pure pyrene derivatives **1(*S*)** and **1(*R*)** covalently attached to the GQDs lead to the formation of chiral GQDs. The structural features of the resultant materials have been studied by a range of analytical and spectroscopic techniques, namely FTIR, XPS, absorption and emission spectroscopy and TGA. Interestingly, these covalent GQDs aggregates, studied by CD, show a Cotton effect in the range of GQDs absorption, thus revealing an efficient chirality transfer from the chiral moieties to the GQDs. The morphology of the GQDs assemblies have been investigated by microscopic techniques, SEM and AFM. The presence of homogeneous height distributions in the AFM analysis and the emission results as well as the confocal images, reveal that hydrogen bonding between the edge amide groups and π-π stacking interactions between GQDs and pyrene-pyrene, are the supramolecular driving forces for the self-aggregation process.

Acknowledgements

This work was financially supported by the Spanish Ministry of Science and Innovation (projects PID2020-114653RB-I00 and PID2020-115120GB-I00).

Conflict of Interest

The authors declare no conflict of interest.

Data Availability Statement

The data that support the findings of this study are available in the supplementary material of this article.

Keywords: Chirality · Fluorescence · Graphene Quantum Dots · Pyrene · Self-Aggregation

[1] a) Y. Luo, X. Yan, J. Zhang, B. Li, Y. Wu, Q. Lu, C. Jin, X. Zhang, X. Ren, *Nanoscale* **2018**, *10*, 9212–9217; b) G. Bottari, M. A. Herranz, L. Wibmer, M. Volland, L. Rodríguez-Pérez, D. M. Guldi, A. Hirsch, N. Martín, F. D'Souza, T. Torres, *Chem. Soc. Rev.* **2017**, *46*, 4464–4500; c) A. K. Geim, K. S. Novoselov, *Nat. Mater.* **2007**, *6*, 183–191; d) F. Bonaccorso, L. Colombo, G. Yu, M. Stoller, V. Tozzini, A. C. Ferrari, R. S. Ruoff, V. Pellegrini, *Science* **2015**, *347*, 1246501; e) K. S. Novoselov, A. K. Geim, S. V. Morozov, D. Jiang, Y. Zhang, S. V. Dubonos, I. V. Grigorieva, A. A. Firsov, *Science* **2004**, *306*, 666–669.

[2] a) K. Dirian, M. A. Herranz, G. Katsukis, J. Malig, L. Rodríguez-Pérez, C. Romero-Nieto, V. Strauss, N. Martín, D. M. Guldi, *Chem. Sci.* **2013**, *4*, 4335–4353; b) K. P. Loh, Q. Bao, G. Eda, M. Chhowalla, *Nat. Chem.* **2010**, *2*, 1015–1024.

[3] S. Li, L. Li, H. Tu, H. Zhang, D. S. Silvester, C. E. Banks, G. Zou, H. Hou, X. Ji, *Mater. Today* **2021**, *51*, 188–207.

[4] Z. Zhang, J. Zhang, N. Chen, L. Qu, *Energy Environ. Sci.* **2012**, *5*, 8869–8890.

[5] a) Y. Yan, J. Gong, J. Chen, Z. Zeng, W. Huang, K. Pu, J. Liu, P. Chen, *Adv. Mater.* **2019**, *31*, 1808283; b) S. Zhu, J. Zhang, C. Qiao, S. Tang, Y. Li, W. Yuan, B. Li, L. Tian, F. Liu, R. Hu, H. Gao, H. Wei, H. Zhang, H. Sun, B. Yang, *Chem. Commun.* **2011**, *47*, 6858–6860; c) L.-s. Li, X. Yan, *J. Phys. Chem. Lett.* **2010**, *1*, 2572–2576; d) L. A. Ponomarenko, F. Schedin, M. I. Katsnelson, R. Yang, E. W. Hill, K. S. Novoselov, A. K. Geim, *Science* **2008**, *320*, 356–358.

[6] X. Yan, X. Cui, L.-s. Li, *J. Am. Chem. Soc.* **2010**, *132*, 5944–5945.

[7] F. Liu, M.-H. Jang, H. D. Ha, J.-H. Kim, Y.-H. Cho, T. S. Seo, *Adv. Mater.* **2013**, *25*, 3657–3662.

[8] a) X. Tan, Y. Li, X. Li, S. Zhou, L. Fan, S. Yang, *Chem. Commun.* **2015**, *51*, 2544–2546; b) X. T. Zheng, A. Ananthanarayanan, K. Q. Luo, P. Chen, *Small* **2015**, *11*, 1620–1636.

[9] A. Ambrosi, C. K. Chua, A. Bonanni, M. Pumera, *Chem. Rev.* **2014**, *114*, 7150–7188.

[10] Y. Yan, J. Chen, N. Li, J. Tian, K. Li, J. Jiang, J. Liu, Q. Tian, P. Chen, *ACS Nano* **2018**, *12*, 3523–3532.

[11] L. Tang, R. Ji, X. Cao, J. Lin, H. Jiang, X. Li, K. S. Teng, C. M. Luk, S. Zeng, J. Hao, S. P. Lau, *ACS Nano* **2012**, *6*, 5102–5110.

[12] Z.-W. Gao, Y. Wang, H. Liu, J. Sun, J. Kim, Y. Li, B. Xu, W. C. H. Choy, *Adv. Funct. Mater.* **2021**, *31*, 2101438.

[13] J. Wang, H. Yan, Z. Liu, Z. Wang, H. Gao, Z. Zhang, B. Wang, N. Xu, S. Zhang, X. Liu, R. Zhang, X. Wang, G. Zhang, L. Zhao, K. Liu, X. Sun, *Nanoscale* **2018**, *10*, 19612–19620.

[14] Z.-b. Qu, W.-J. Feng, Y. Wang, F. Romanenko, N. A. Kotov, *Angew. Chem. Int. Ed.* **2020**, *59*, 8542–8551; *Angew. Chem.* **2020**, *132*, 8620–8629.

[15] a) K. Kato, K. Takaba, S. Maki-Yonekura, N. Mitoma, Y. Nakanishi, T. Nishihara, T. Hatakeyama, T. Kawada, Y. Hijikata, J. Pirillo, L. T. Scott, K. Yonekura, Y. Segawa, K. Itami, *J. Am. Chem. Soc.* **2021**, *143*, 5465–5469; b) I. Matsumoto, R. Sekiya, T. Haino, *Angew. Chem. Int. Ed.* **2021**, *60*, 12706–12711; *Angew. Chem.* **2021**, *133*, 12816–12821.

[16] Y. Uemura, K. Yamato, R. Sekiya, T. Haino, *Angew. Chem. Int. Ed.* **2018**, *57*, 4960–4964; *Angew. Chem.* **2018**, *130*, 5054–5058.

[17] a) J. M. Fernández-García, P. Izquierdo-García, M. Buendía, S. Filippone, N. Martín, *Chem. Commun.* **2022**, *58*, 2634–2645; b) J. M. Fernández-García, P. J. Evans, S. Filippone, M. A. Herranz, N. Martín, *Acc. Chem. Res.* **2019**, *52*, 1565–1574.

[18] a) P. Izquierdo-García, J. M. Fernández-García, I. Fernández, J. Perles, N. Martín, *J. Am. Chem. Soc.* **2021**, *143*, 11864–11870; b) J. Urieta-Mora, M. Krug, W. Alex, J. Perles, I. Fernández, A. Molina-Ontoria, D. M. Guldi, N. Martín, *J. Am. Chem. Soc.* **2020**, *142*, 4162–4172; c) D. Reger, P. Haines, F. W. Heinemann, D. M. Guldi, N. Jux, *Angew. Chem. Int. Ed.* **2018**, *57*, 5938–5942; *Angew. Chem.* **2018**, *130*, 6044–6049; d) S. H. Pun, Q. Miao, *Acc. Chem. Res.* **2018**, *51*, 1630–1642; e) K. Kato, Y. Segawa, L. T. Scott, K. Itami, *Angew. Chem. Int. Ed.* **2018**, *57*, 1337–1341; *Angew. Chem.* **2018**, *130*, 1351–1355; f) J. M. Fernández-García, P. J. Evans, S. Medina Rivero, I. Fernández, D. García-Fresnadillo, J. Perles, J. Casado, N. Martín, *J. Am. Chem. Soc.* **2018**, *140*, 17188–17196; g) P. J. Evans, J. Ouyang, L. Favereau, J. Crassous, I. Fernández, J. Perles, N. Martín, *Angew. Chem. Int. Ed.* **2018**, *57*, 6774–6779; *Angew. Chem.* **2018**, *130*, 6890–6895; h) C. M. Cruz, I. R. Márquez, I. F. A. Mariz, V. Blanco, C. Sánchez-Sánchez, J. M. Sobrado, J. A. Martín-Gago, J. M. Cuerva, E. Maçôas, A. G. Campaña, *Chem. Sci.* **2018**, *9*, 3917–3924; i) M. Rickhaus, M. Mayor, M. Juríček, *Chem. Soc. Rev.* **2017**, *46*, 1643–1660; j) K. Kawasumi, Q. Zhang, Y. Segawa, L. T. Scott, K. Itami, *Nat. Chem.* **2013**, *5*, 739–744.

[19] a) A. Döring, E. Ushakova, A. L. Rogach, *Light: Sci. Appl.* **2022**, *11*, 75; b) N. Suzuki, Y. Wang, P. Elvati, Z.-B. Qu, K.

Kim, S. Jiang, E. Baumeister, J. Lee, B. Yeom, J. H. Bahng, J. Lee, A. Violi, N. A. Kotov, *ACS Nano* **2016**, *10*, 1744–1755.
[20] M. Vázquez-Nakagawa, L. Rodríguez-Pérez, M. A. Herranz, N. Martín, *Chem. Commun.* **2016**, *52*, 665–668.
[21] S. Nishitani, R. Sekiya, T. Haino, *Angew. Chem. Int. Ed.* **2020**, *59*, 669–673; *Angew. Chem.* **2020**, *132*, 679–683.
[22] W. S. Hummers, R. E. Offeman, *J. Am. Chem. Soc.* **1958**, *80*, 1339.
[23] R. Sekiya, Y. Uemura, H. Murakami, T. Haino, *Angew. Chem. Int. Ed.* **2014**, *53*, 5619–5623; *Angew. Chem.* **2014**, *126*, 5725–5729.
[24] L. Lin, S. Zhang, *Chem. Commun.* **2012**, *48*, 10240–10242.
[25] a) M. Garrido, J. Calbo, L. Rodríguez-Pérez, J. Aragó, E. Ortí, M. A. Herranz, N. Martín, *Chem. Commun.* **2017**, *53*, 12402–12405; b) A. Roth, C. Schierl, A. Ferrer-Ruiz, M. Minameyer, L. Rodríguez-Pérez, C. Villegas, M. A. Herranz, N. Martín, D. M. Guldi, *Chem* **2017**, *3*, 164–173; c) S. S. Gkermpoura, K. D. Papadimitriou, E. N. Skountzos, I. Polyzos, M. G. Pastore Carbone, A. Kotrotsos, V. G. Mavrantzas, C. Galiotis, C. Tsitsilianis, *Nanoscale* **2019**, *11*, 915–931.
[26] T. Scharl, A. Ferrer-Ruiz, A. Saura-Sanmartín, L. Rodríguez-Pérez, M. A. Herranz, N. Martín, D. M. Guldi, *Chem. Commun.* **2019**, *55*, 3223–3226.
[27] M. Garrido, M. K. Volland, P. W. Munich, L. Rodríguez-Perez, J. Calbo, E. Ortí, M. A. Herranz, N. Martín, D. M. Guldi, *J. Am. Chem. Soc.* **2020**, *142*, 1895–1903.
[28] a) K. Kise, S. Ooi, H. Saito, H. Yorimitsu, A. Osuka, T. Tanaka, *Angew. Chem. Int. Ed.* **2022**, *61*, e202112589; *Angew. Chem.* **2022**, *134*, e202112589; b) J. Hoche, H.-C. Schmitt, A. Humeniuk, I. Fischer, R. Mitrić, M. I. S. Röhr, *Phys. Chem. Chem. Phys.* **2017**, *19*, 25002–25015; c) G. K. Bains, S. H. Kim, E. J. Sorin, V. Narayanaswami, *Biochemistry* **2012**, *51*, 6207–6219; d) K. Kalyanasundaram, J. K. Thomas, *J. Am. Chem. Soc.* **1977**, *99*, 2039–2044.
[29] a) G. Fittolani, D. Vargová, P. H. Seeberger, Y. Ogawa, M. Delbianco, *J. Am. Chem. Soc.* **2022**, *144*, 12469–12475; b) S. M. Morrow, A. J. Bissette, S. P. Fletcher, *Nat. Nanotechnol.* **2017**, *12*, 410–419; c) Y. Zhou, R. L. Marson, G. van Anders, J. Zhu, G. Ma, P. Ercius, K. Sun, B. Yeom, S. C. Glotzer, N. A. Kotov, *ACS Nano* **2016**, *10*, 3248–3256; d) A. Insuasty, C. Atienza, J. L. López, N. Martín, *Chem. Commun.* **2015**, *51*, 10506–10509; e) J. L. López, C. Atienza, A. Insuasty, J. López-Andarias, C. Romero-Nieto, D. M. Guldi, N. Martín, *Angew. Chem. Int. Ed.* **2012**, *51*, 3857–3861; *Angew. Chem.* **2012**, *124*, 3923–3927.
[30] A. Sikder, D. Ray, V. K. Aswal, S. Ghosh, *Angew. Chem. Int. Ed.* **2019**, *58*, 1606–1611; *Angew. Chem.* **2019**, *131*, 1620–1625.
[31] Y. Wang, A. Hu, *J. Mater. Chem. C* **2014**, *2*, 6921–6939.

Manuscript received: August 3, 2022
Accepted manuscript online: August 31, 2022
Version of record online: September 27, 2022